Наносистеми, наноматеріали, нанотехнології
Nanosistemi, Nanomateriali, Nanotehnologii
2017, т. 15, № 4, сс. 675–686

PACS numbers: 61.05.cp, 61.05.Qr, 68.37.Lp, 81.07.-b, 81.16.-c, 82.45.Yz, 82.47.Aa

Plate-Like $LiFePO_4$ Nanoparticles: Synthesis, Structure, Electrochemistry

V. O. Kotsyubynsky[1], B. K. Ostafiychuk[2], R. P. Lisovsky[1], V. V. Moklyak[2], A. B. Hrubiak[1], I. I. Hryhoruk[1], and Al-Saedi Abdul Halek Zamil[3]

[1]*Vasyl Stefanyk Precarpathian National University, 57 Shevchenko Str., 76018 Ivano-Frankivsk, Ukraine*
[2]*G. V. Kurdyumov Institute for Metal Physics, N.A.S. of Ukraine, 36 Academician Vernadsky Blvd., UA-03142 Kyiv, Ukraine*
[3]*South Ukrainian National Pedagogical University Named After K. D. Ushynsky, 26 Staroportofrankivs'ka Str., 65020 Odesa, Ukraine*

Lithium iron phosphate plate-like particles of 100–150 nm sizes and to 10 nm thickness have been obtained by hydrothermal synthesis. It has been aim to investigate influence of ethylene glycol relative content and reaction medium temperature on the obtained-materials' phase composition, crystalline and magnetic microstructure, surface condition and electrical properties. As determined, there is correlation between the materials' morphology and their electrochemical properties. The reducing of a particle size and agglomeration degree leads to specific capacity growing for lithium power sources with cathodes based on synthesized materials.

Гідротермічною синтезою одержано платівчасті частинки літій-залізного фосфату розмірами у 100–150 нм і товщиною до 10 нм. Метою було дослідження впливу відносного вмісту етиленгліколю та температури реакційного середовища на фазовий склад одержаних матеріалів, їхні кристалічну та магнетну мікроструктури, стан поверхні й електричні властивості. Визначено, що є кореляція між морфологією матеріалів та їхніми електрохемічними властивостями. Зменшення розміру частинок і ступеня аґломерації приводить до підвищення питомої місткости літійових джерел живлення з катодами на основі синтезованих матеріялів.

Гидротермальным синтезом получены пластинчатые частицы литий-железного фосфата размерами 100–150 нм и толщиной до 10 нм. Це-

лью было исследование влияния относительного содержания этиленгликоля и температуры реакционной среды на фазовый состав полученных материалов, их кристаллическую и магнитную микроструктуры, состояние поверхности и электрические свойства. Установлено, что имеется корреляция между морфологией материалов и их электрохимическими свойствами. Уменьшение размера частиц и степени агломерации приводит к увеличению удельной ёмкости литиевых источников энергии с катодами на основе синтезированных материалов.

Key words: lithium iron phosphate, nanoparticles, morphology, conductivity, cathode, lithium power sources.

Ключові слова: літій-залізний фосфат, наночастинки, морфологія, провідність, катода, літійові джерела живлення.

Ключевые слова: литий-железный фосфат, наночастицы, морфология, проводимость, катод, литиевые источники питания.

(Received 10 April, 2017)

1. INTRODUCTION

Specific energy density of lithium iron phosphate ($LiFePO_4$) is compared to best commercial compounds $LiCoO_2$, $LiNiO_2$, $LiMn_2O_4$. At the same time, the material is characterized by a slower rate of capacity loss, high reversible capacity of about 170 A·h/kg at an open-circuit voltage of 3.45 V versus Li/Li^+ (Fe^{2+}/Fe^{3+} redox couple) with long cycle ability (typically more than 2.000 charge–discharge cycles at 1°C current rate with approximately 80% capacity saving) [1]. The other advantages are high charge–discharge current rates up to 10°C, good safety owing to high thermal stability, flat charge/discharge curves (reversible $LiFePO_4/FePO_4$-phases' transformation), low cost of production and utilization. The key point is a high performance of cathode material but low electronic conductivity and one-dimensional diffusion of lithium ions require small particle sizes and shape control during the synthesis. The main imperfection of $LiFePO_4$ is low conductivity (about 10^{-9} S/cm in comparison with 10^{-4} S/cm for $LiCoO_2$ and 10^{-6} S/cm for $LiCoO_2$), which complicates a theoretical capacity obtainment at high discharge current rates [2, 3]. Another problem is a one-dimensional slow diffusion of Li^+ ions (10^{-13}–10^{-14} cm^2/s for $LiFePO_4$ and about 10^{-16} cm^2/s for $FePO_4$). $LiFePO_4$ particles' carbon coating or non-stoichiometric material synthesis is usually used for conductivity increasing [2, 4–6]. Another approach consists of particles sizes reduction for the lengths of ionic and electronic transport reducing [7].

Alongside with it, high specific surface area and low coordinated

surface atoms may cause particles agglomeration and surface reactions. As a result, the properties of the $LiFePO_4$ crucially depend on the synthesis route and the modification of it allows a predictable change of material morphological and electrical characteristics. There is a wide range of different approaches to $LiFePO_4$ obtaining: solid-state methods, sol–gel route, microemulsion method [8–10].

A special place is taken by hydrothermal synthesis that allows to control additionally a reaction medium during the process and to influence actively the particles morphology [11].

The objective of this research is to improve the plate-like $LiFePO_4$ nanoparticles obtaining method by hydrothermal synthesis and to find regularities between the materials' electrical and morphological properties and their electrochemical performance.

2. MATERIALS AND METHODS

Nanoparticles of $LiFePO_4$ were prepared according to the following procedure [12]: 1 mole/L H_3PO_4 was mixed with ethylene glycol at a different ratio with the next 1 mole/L LiOH aqueous solution dropwise addition under mechanical stirring. At the last stage, 3 mole/L $FeSO_4 \cdot 7H_2O$ aqueous solution was added to a white suspension formed after the neutralization reaction. Green coloured resulting suspension was sealed into a 0.5 L magnetic mixed autoclave. The autoclave was heated to a temperature of 200–240°C at heating rate of 3–4°C/min with the exposure for 1–5 hours under stirring. Thereafter, the autoclave was cooled to room temperature. The colloidal suspension was collected *via* centrifuge and washed with distilled water up to neutral pH. The obtained materials were dried under vacuum at 70–80°C for 8 h.

The two systems (S1 and S2) of materials were synthesized at those conditions. S1 series samples were differed by their relative content of ethylene glycol in the initial mixture and were obtained at 240°C (Table). Samples series S2 were obtained at 67 vol.% ethylene glycol relative content after exposure at 2 different temperatures, 200 and 220°C. For carbon coating formation, the S1-3 sample were mixed with 17 wt.% of glucose and then sintered at 400°C

TABLE. S1 samples synthesis conditions.

Sample	Ethylene glycol relative content, vol. %	pH of initial mixture
S1-1	40	3.9
S1-2	57	4.4
S1-3	67	4.6
S1-4	77	5.0

for 1 h under argon atmosphere with a heating rate of 5–6°C/min.

Diffraction patterns were obtained with diffractometer DRON-4-07 (CuK_α radiation). Bragg–Brentano geometry type and a NiK_β-filter were applied. A quantitative analysis was done with a full pattern Rietveld refinement procedure using FullFrof Suite Program [12 XRD measurements were collected in a 2θ range of 16–65°.

High-resolution transmission electron microscopy (HRTEM) images were obtained by a microscope FEI Tecnai Orisis TEM/STEM 80–200 at a 200 kV. The samples were ultrasonically mixed in isopropyl alcohol and deposited on silica substrates.

The Mössbauer spectra were measured with a MS-1104Em spectrometer using a ^{57}Co γ-ray source and calibrated at room temperature with α-Fe as a standard (linewidth 0.29 mm/s). The isomer shifts (δ) are relative to Fe metal. The model fitting was performed using Mosswin 3.0 software.

The Brunauer–Emmett–Teller (BET) specific surface areas of the samples were measured by Nitrogen adsorption/desorption methods at 77 K with a Quantachrome NOVA 2200e analyser.

Electrochemical impedance spectroscopy with Autolab PGSTAT 12 galvanostat/potentiostat (conventional four-electrode configuration) was used to explore the conductivity of the obtained samples over the frequency range 0.01 Hz–100 kHz.

Electrochemical lithium intercalation/deintercalation tests were performed in Swagelok-type cells assembled in an argon-filled dry glow box. The negative electrode was a lithium metal foil. The electrolyte was 1 mole/L $LiBF_4$ dissolved in γ-butyrolactone. Cathode mixture consisted of the obtained materials, black carbon and PVDF (mass ratio 85:10:5) in acetone was prepared in the paste form. The positive electrode was Ni grid coated by cathode mixture. The cell was charged and discharged at a rate of C/10. All electrochemical tests were carried out at room temperature.

3. RESULTS AND DISCUSSION

According to XRD data (Fig. 1), S1-2 and S1-3 materials were a pure $LiFePO_4$ [14].

A presence of $Fe_2P_2O_7$ (more than 55 wt.%) impurity phase for S1-4 sample has been observed. The most interesting is a S1-1 sample. The intensive peak at $2\theta = 17.37°$ on the XRD pattern for this sample was originally identified as a yield of $LiFeP_2O_7$ phase presence. However, in $LiFeP_2O_7$ compound, the iron is in a Fe^{3+} state. As a result, it leads to the predicted differences between the contributions of $LiFeP_2O_7$ and $LiFePO_4$ phases to the Mössbauer spectra integral intensity (Fig. 2). A doublet component presence with

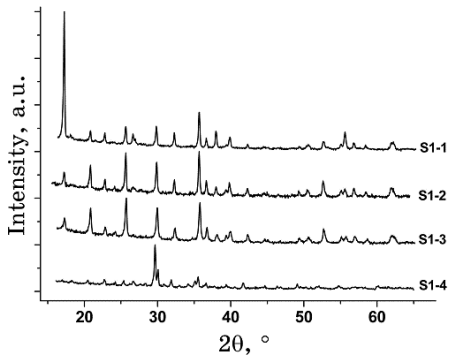

Fig. 1. XRD patterns of S1 system samples.

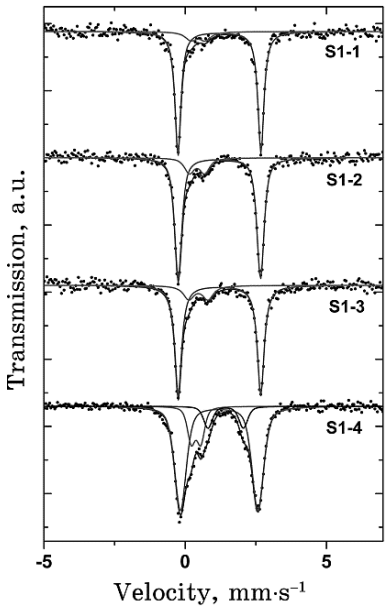

Fig. 2. Mössbauer spectra of S1 system samples.

quadrupole splitting (Δ) in particular is less than 1 mm/s and could be considered as an evidence of $LiFeP_2O_7$ phase. At the same time, Mössbauer spectra of S1-1 sample consist of two doublet components.

A dominating doublet component with integral intensity relative content of about 92% corresponds to $LiFePO_4$ ($\Delta = 2.93$ mm/s, $\delta = 1.21$ mm/s). The obtained parameters of Mössbauer spectra are very close to the literature data for $LiFePO_4$ [15]. The integral relative intensity of the second doublet component ($\Delta = 0.54$ mm/s,

$\delta = 0.42$ mm/s) does not exceed 8%; so, the assumption about $LiFeP_2O_7$ phase availability has been neglected.

Another working hypothesis is a sharp anisotropy of $LiFePO_4$ particles' shape that causes redistribution of diffraction peaks intensity. In the case of plate-like particles, the peak at $2\theta = 17.37°$ will correspond to (200) reflex of the $LiFePO_4$ structure (result of XRD pattern modelling with the use of PowderCell software and Rietveld–Toraya model) [16]. This assumption is confirmed by TEM investigations (Fig. 3).

The S1-1 sample is formed by separated plate-like particles of $LiFePO_4$ with the sizes of 200–300 nm and of thickness to 20–30 nm with crystal orientation along the bc facet. The particles lamellar morphology also happens in S1-2 and S1-3 materials, but this form is not dominant, and the majority of particles are prismatic (Fig. 3). It can be assumed that the ethylene glycol molecules after absorption on the $LiFePO_4$ nuclei prevent crystal growth. Similar results (preferred crystal orientation with a (200) texture) were ob-

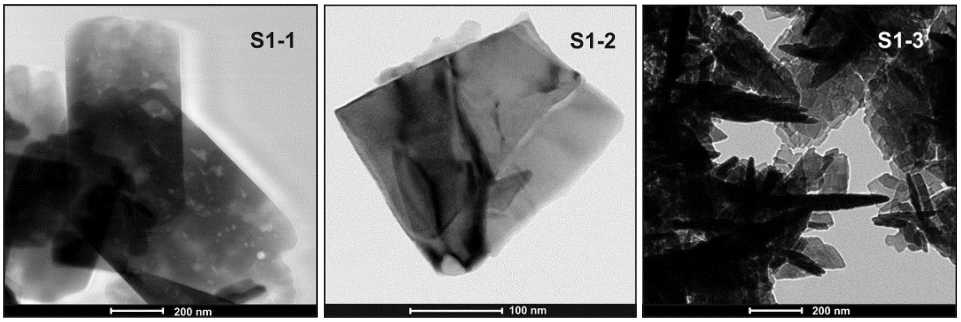

Fig. 3. TEM picture of S1 system samples.

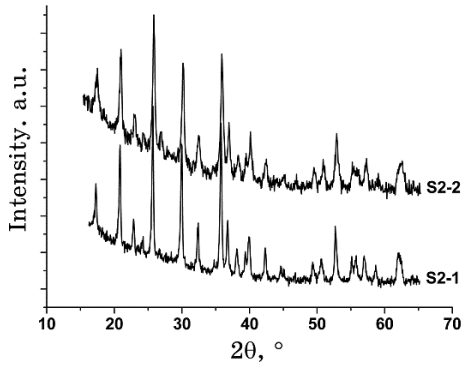

Fig. 4. XRD patterns of S2 system samples.

tained in [17] in a case of $LiFePO_4$ hydrothermal synthesis.

One of the biggest problems in $LiFePO_4$ synthesis is to determine the conditions for a pure phase obtaining and to prevent oxidation of Fe^{2+} to Fe^{3+}. The presence of Fe^{3+} is systematically detected by Mössbauer spectroscopy measurements of $LiFePO_4$ nanoparticles at the absence of additional iron-containing phase [15]. One of the reasons for this phenomenon is the process of surface iron oxidation in the oxygen-containing medium [18]. Small contents of Fe^{3+} ions in $LiFePO_4$ could be caused by the Li^+ ions' substitution for Fe^{2+} sites with the next oxidation of some Fe^{2+} to Fe^{3+} for charge compensation. Additional electron density on the lithium sites was fixed in [19]. The substitution does not cause significant structural changes because the ionic radii of Fe^{2+} and Fe^{3+} are close (92 and 79 pm, respectively) and phosphorus-oxygen [PO_4] polyhedra are strongly bonded. Formation of Fe^{3+} ions can be stimulated by the aqueous medium too [20].

Mössbauer spectroscopy is a good technique to investigate local electronic structure and coordination of Fe ions. The establishment of Fe^{3+} ions coordination type from the isomer shift calibration is possible. The following criteria can be used: Fe^{3+} (tetrahedral coordinated) $< \delta = 0.3–0.4$ mm/s $< Fe^{3+}$ (octahedral coordinated) [15]. This value suggests that a minor doublet component is a result of Fe^{3+} ions presence in both coordination states. This estimation can be indirect evidence of the Fe^{3+} ions presence on disordered surface shell of the $LiFePO_4$ particles.

Mössbauer spectra of S1-2 and S1-3 materials have the composition similar to S1-1 with the relative content of Fe^{3+} ion of 11 and 13%, respectively. From this, it follows that $LiFePO_4$ yield decreases with the increasing pH of initial precursor mixture. The result obtained is contrary to the data about an increase of the lithium iron phosphate yield with pH growth linked to $LiFePO_4$ solubility enlarging in acidic condition under excessive pressure and at high temperature [17].

With XRD patterns of S2 system samples obtained at hydrothermal treatment temperature of 200 and 220°C at the same ethylene glycol contents (marked S2-1 and S2-2), no additional phases except $LiFePO_4$ have been fixed in either case (Fig. 4). The average size of coherent scattering regions some decrease (from 16 to 14 nm) with the synthesis temperature elevation is possible. This result correlates to the adsorption porosimetry data: the specific surface areas of the S2-1 and S2-2 materials are 17 and 13 m^2/g, respectively.

The relative content of Fe^{3+} ions for S2-1 and S2-2 materials is unexpectedly high, *i.e.*, 18 and 21%, respectively (Fig. 5). The isomer shift and quadruple splitting of minor doublet component for S2-1 and S2-2 are very close to the characteristic parameters of S1

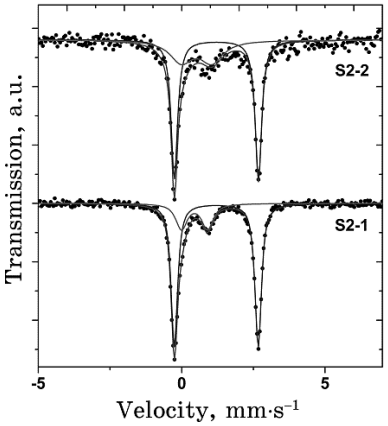

Fig. 5. Mössbauer spectra of S2 system samples.

system samples. At the same time, some morphological differences have been found. For S2-1 sample, agglomerates with the sizes of 0.3–1.0 μm consisting of ordered separate prismatic particles of 100–150 nm are typical. For S2-2 sample, such ordering has not been observed, and agglomerates with the close sizes are formed by primary particles with different sizes and shapes (Fig. 6).

The increasing of Fe^{3+} ions to 25% was observed after carbon coating procedure for S1-3 sample. Mössbauer spectra parameters for the minor doublet component were as follow: $\Delta = 0.84$ mm/s and $\delta = 0.43$ mm/s (Fig. 7). Those parameters were close to $Fe_4P_6O_{21}$ ferric pyrophosphate characteristics ($\Delta = 0.80$ mm/s and $\delta = 0.42$ mm/s), but that compound formation is hardly probable [21].

The frequency dependences of the complex conductivity for S1-3 and S1-3/carbon samples were obtained by the impedance spectroscopy method (Fig. 8). The curves for both samples can be divided into two regions: the linear frequency independent part and the second one where conductivity increases with frequency enlarging. The obtained dispersion curves were approximated by Jonscher's power law [22]:

$$\sigma(\omega) = \sigma_{dc}\left[1 + \left(\frac{\omega}{\omega_h}\right)\right]^s, \qquad (1)$$

where σ_{dc} is the frequency independent part of conductivity, ω_h is the hopping frequency of the charge carriers, and s is an exponent parameter characterizing the deviation of the system from the Debye-type state (of $s = 1$). The parameter s is a measure of the interionic–environmental coupling strength and, for most cases, is in the range of $0 < s < 1$. Alongside with it, there is no physical reasons

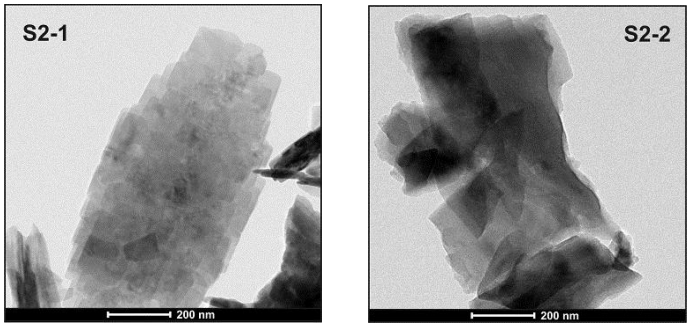

Fig. 6. TEM picture of S2 system samples.

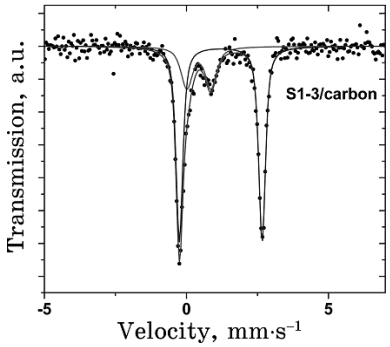

Fig. 7. Mössbauer spectra of S1-3/carbon sample.

inability for the parameter s to take on values above 1 [23]. Jonscher's law is performed for a wide range of the material types—from disordered semiconductors to conducting polymers and ion glasses. This qualitative characteristic of the universal response is relevant to material morphology and spatial structure of the conduction network. In our case, the parameter s was 1.34 ± 0.02 and 1.37 ± 0.02 for S1-3 and S1-3/carbon materials, respectively.

A model of electric-charge transfer in the disordered matter based on the distribution of the length of accessible conduction paths with power exponent $s > 1$ larger was proposed in [24]. For carbon-containing composite, dc-conductivity σ_{dc} have been increased to $(6.1 \pm 0.8) \cdot 10^{-7}$ Sm·m^{-1} from $(1.9 \pm 0.6) \cdot 10^{-6}$ Sm·m^{-1} for initial S1-3 material. Average hopping frequency ω_h of charge carriers was increased from $(3.7 \pm 0.4) \cdot 10^3$ to $(5.1 \pm 1.8) \cdot 10^3$ Hz. In possible qualitative model, composite material is that of a grid of random oriented chains of various lengths that consists of $LiFePO_4$ particles interconnected by carbon bridges with conformational dis-

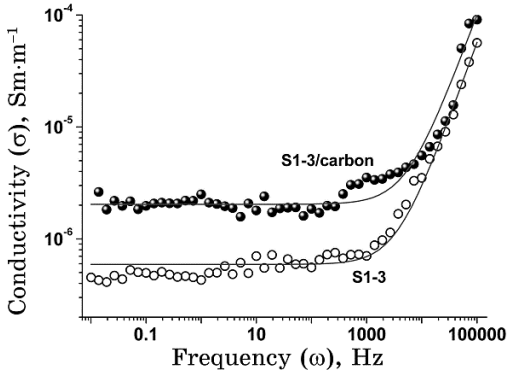

Fig. 8. Frequency dependency of S1-3 and S1-3/carbon samples electrical conductivity (solid lines represent fitting results).

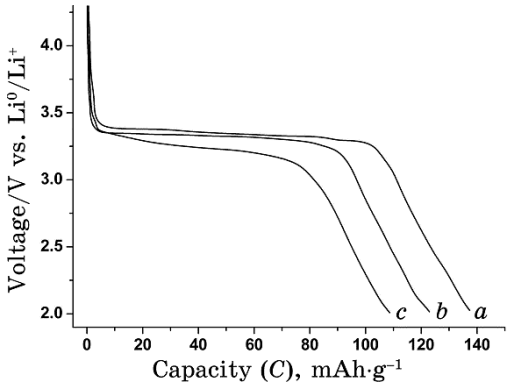

Fig. 9. Discharge voltage profiles using the $LiFePO_4/LiBF_4$–γ-butyrolactone/Li cell at room temperature for various cathode materials: (*a*) S1-3/carbon, (*b*) S1-3, and (*c*) S2-1.

order. Electronic transport in olivine $LiFePO_4$ is caused by polaron hopping. Thus, in carbon-containing composite, trapping was realized both along chain (intrachain transfer) and over cross-connected chains at the increasing of hops probability with grid density enlarging.

Obtained discharge voltage profiles of the $LiFePO_4$ cathode material appear to be a typical voltage plateau (at about 3.4 V *vs.* Li^0/Li^+) attributed to the coexistence of two isostructural similar phases—$LiFePO_4$ and $FePO_4$ (Fig. 9). The carbon-containing material exhibited a maximal capacity of about 140 mA·h/g in the voltage range of 2.2–4.0 V. In comparison, the initial S1-3 material under the same conditions demonstrates a lower specific capacity of about 120 mA·h/g. The plateau voltages for S1-3 and S1-3 /carbon are

very close, but the width of the plateau for composite material is larger. For S2-1 material, a smaller plateau is characterized by some slope that is probably connected to diffuse distances increasing during Li intercalation with the particles (agglomerates) sizes growing. Indistinctive long 'tails' was observed on the voltage–capacity curves during the last discharge step. For all cases, we connect it with the relatively high inner resistance of the cathodes.

4. CONCLUSIONS

Nanosize $LiFePO_4$ particles have been prepared by hydrothermal route using ethylene glycol as morphology predicted surfactant. The plate-like $LiFePO_4$ particles with a minimal Fe^{3+} ions content have been obtained with 40 vol.% ethylene glycol relative content at 240°C. $Fe_2P_2O_7$ impurity phase formation at 77 vol.% ethylene glycol relative content is fixed. As determined, the changes of the reaction medium temperature in a range of 200–240°C have had no impact on a phase state of the material and on the average size of the primary prismatic particles (100–150 nm). The ordering character of the agglomerates' formation is observed at the temperature of 200°C. The frequencies dependences of conductivity for obtained materials and $LiFePO_4$/carbon composite have been analysed with the using of electric-charge transfer in disordered matter formalism. The electrochemical properties of the $LiFePO_4$ cathodes depend on the agglomerate sizes and the presence of carbon coating.

ACKNOWLEDGMENT

The publication contains the results of studies conducted under the President's of Ukraine grant for competitive projects of the State Fund for Fundamental Research.

REFERENCES

1. A. Kumar, R. Thomas, N. K. Karan, J. J. Saavedra-Arias, M. K. Singh, S. B. Majumder, and R. S. Katiyar, *J. Nanotechnol.*, **2009**, (2009): ID 176517; doi: 10.1155/2009/176517.
2. M. Park, X. Zhang, M. Chung, G. B. Less, and A. M. Sastry, *J. Power Sources*, **195**, No. 24: 7904 (2010).
3. G. T.-K. Fey, Y. G. Chen, and H.-M. Kao, *J. Power Sources*, **189**, No. 1: 169 (2009).
4. G. K. P. Dathar, D. Sheppard, K. J. Stevenson, and G. Henkelman, *Chem. Mater.*, **23**, No. 17: 4032 (2011).
5. C. R. Sides, F. Croce, V. Y. Young, C. R. Martin, and B. Scrosati, *Electrochem. Solid-State Lett.*, **8**, No. 9: A484 (2005).

6. B. Kang and G. Ceder, *Nature*, **458**: 190 (2009).
7. A. Yamada, S. C. Chung, and K. Hinokuma, *J. Electrochem. Soc.*, **148**, No. 3: A224 (2001).
8. H. C. Kang, D. K. Jun, B. Jin, E. M. Jin, K. H. Park, H. B. Gu, and K. W. Kim, *J. Power Sources*, **179**, No. 1: 340 (2008).
9. S. Beninati, L. Damen, and M. Mastragostino, *J. Electrochem. Soc.*, **194**, No. 2: 1094 (2009).
10. Z. Xu, L. Xu, Q. Lai, and X. Ji, *Mater. Chem. Phys.*, **105**, No. 1: 80 (2007).
11. B. Pei, H. Yao, W. Zhang, and Z. Yang, *J. Electrochem. Soc.*, **220**: 317 (2012).
12. V. Kotsyubynsky, A. S. A. H. Zamil, V. Moklyak, and R. Lisovsky, *2014 IEEE International Conference on Oxide Materials for Electronic Engineering–OMEE 2014* (*Lviv, 26–30 May, 2014*), p. 100; DOI: 10.1109/OMEE.2014.6912359.
13. J. Rodriguez-Carvajal, *Newsletter*, **26**: 12 (2001).
14. V. A. Streltsov, E. L. Belokoneva, V. G. Tsirelson, and N. K. Hansen, *Acta Crystallogr. Sect. B: Struct. Sci.*, **49**, No. 2: 147 (1993).
15. K. Hirose, T. Honma, Y. Doi, Y. Hinatsu, and T. Komatsu, *Solid State Commun.*, **146**, No. 5: 273 (2008).
16. W. Kraus and G. Nolze, *J. Appl. Crystallogr.*, **29**, No. 3: 301 (1996).
17. K. Kanamura, S. Koizumi, and K. Dokko, *J. Mater. Sci.*, **43**, No. 7: 2138 (2008).
18. K. Zaghib, A. Mauger, F. Gendron, and C. M. Julien, *Chem. Mater.*, **20**, No. 2: 462 (2007).
19. J. Chen and M. S. Whittingham, *Electrochem. Commun.*, **8**, No. 5: 855 (2006).
20. W. Porcher, P. Moreau, B. Lestriez, S. Jouanneau, F. Le Cras, and D. Guyomard, *Ionics*, **14**, No. 6: 583 (2008).
21. K. Bazzi, M. Nazri, V. M. Naik, V. K. Garg, A. C. Oliveira, P. P. Vaishnava, and R. Naik, *J. Power Sources*, **306**: 17 (2016).
22. J. K. Lee, H. W. Park, H. W. Choi, J. E. Kim, S. J. Kim, and Y. S. Yang, *J. Korean Phys. Soc.*, **47**: S267 (2005).
23. B. Louati, M. Gargouri, K. Guidara, and T. Mhiri, *J. Phys. Chem. Solids*, **66**, No. 5: 762 (2005).
24. A. N. Papathanassiou, I. Sakellis, and J. Grammatikakis, *Appl. Phys. Lett.*, **91**, No. 12: 122911 (2007); doi: 10.1063/1.2779255.